A direct estimate of poleward volume, heat, and freshwater fluxes at 59.5°N between Greenland and Scotland

T. Rossby, Gilles Reverdin, Léon Chafik, Henrik Søiland

AGU PUBLICATIONS

JGR

Journal of Geophysical Research: Oceans

RESEARCH ARTICLE

10.1002/2017JC012835

Key Points:
- Currents and transports can be measured to great accuracy from vessels operating at high speed
- Accurate estimates of the MOC, heat, and freshwater fluxes
- Two ADCP studies, 13 years apart, give almost the same upper ocean transport between Greenland and Scotland with the more recent period slightly greater

Correspondence to:
T. Rossby,
trossby@gso.uri.edu

Citation:
Rossby, T., G. Reverdin, L. Chafik, and H. Søiland (2017), A direct estimate of poleward volume, heat, and freshwater fluxes at 59.5°N between Greenland and Scotland, *J. Geophys. Res. Oceans*, *122*, 5870–5887, doi:10.1002/2017JC012835.

Received 26 FEB 2017
Accepted 27 JUN 2017
Accepted article online 5 JUL 2017
Published online 25 JUL 2017

A direct estimate of poleward volume, heat, and freshwater fluxes at 59.5°N between Greenland and Scotland

T. Rossby[1], Gilles Reverdin[2], Leon Chafik[3], and Henrik Søiland[4]

[1]Graduate School of Oceanography, University of Rhode Island, Kingston, Rhode Island, USA, [2]LOCEAN, Sorbonne Universites, UPMC/CNRS/IRD/MNHN, Paris, France, [3]Geophysical Institute, Bjerknes Center for Climate Research, University of Bergen, Bergen, Norway, [4]Institute of Marine Research, Bjerknes Center for Climate Research, Bergen, Norway

Abstract The meridional overturning circulation (MOC) in the North Atlantic plays a major role in the transport of heat from low to high latitudes. In this study, we combine recent measurements of currents from the surface to >700 m from a shipboard acoustic Doppler current profiler with Argo profiles (to 2000 m) to estimate poleward volume, heat, and freshwater flux at 59.5°N between Greenland and Scotland. This is made possible thanks to the vessel Nuka Arctica that operates on a 3 week schedule between Greenland and Denmark. For the period late 2012 to early 2016, the deseasoned mean meridional overturning circulation reaches a 18.4 ± 3.4 Sv maximum at the $\sigma_\theta = 27.55$ kg m^{-3} isopycnal, which varies in depth from near the surface in the western Irminger Sea to 1000 m in Rockall Trough. The total heat and freshwater fluxes across 59.5°N = 399 ± 74 TW and −0.20 ± 0.04 Sv, where the uncertainties are principally due to that of the MOC. Analysis of altimetric sea surface height variations along exactly the same route reveals a somewhat stronger geostrophic flow north during this period compared to the 23 year mean suggesting that for a long-term mean the above flux estimates should be reduced slightly to 17.4 Sv, 377 TW, and −0.19 Sv, respectively, with the same estimate uncertainties. The ADCP program is ongoing.

1. Introduction and Motivation for the Study

The North Atlantic Ocean between Greenland and Europe is traversed by a strong poleward flow of warm saline water that feeds the convective production of intermediate and deep waters in the Labrador, Irminger, and Nordic Seas, respectively. In this study, we will use a new archive of directly measured currents to quantify these flows and to address whether such measurements can inform us on the space-time variability of warm water flow through these regions. This water owes its heat and saltiness to its tropical origins and its rapid transit north along the Gulf Stream and North Atlantic Current (NAC). This flow is also known as a link in the upper branch of the meridional overturning circulation (MOC). After crossing the mid-Atlantic Ridge, a major fraction of the NAC turns north in the southern Iceland Basin with some water curving northwest toward the Reykjanes Ridge (hereafter the Ridge) and Irminger Sea, some continuing north through the Iceland Basin toward the Faroe-Shetland Channel and the Iceland-Faroe Ridge, and some continuing east toward Rockall Trough [e.g., *Chafik et al*., 2014; *García-Ibáñez et al*., 2015; *Mercier et al*., 2015; *Daniault et al*., 2016]. These multiple pathways eventually "come together" to meet the demand for warm salty water in two different convective regions, namely the Nordic Seas, where deep North Atlantic Water is ultimately formed, and the Labrador Sea, where water of intermediate density is formed.

Charting the path of especially the Labrador Sea branch and its transport has proven to be quite a challenge; most hydrographic studies picture North Atlantic water flowing cyclonically around the northern North Atlantic crossing the Ridge into the Irminger Sea [e.g., *McCartney and Talley*, 1984; *Krauss*, 1986; *Heywood et al*., 1994]. In contrast, *Ivers* [1975] shows the warm North Atlantic water flowing back south along the eastern slope of the Ridge before turning back north along its western slope. This latter view of how topography can shape or constrain the mean circulation has also been seen in several Lagrangian studies [e.g., *Lavender et al*., 2000, 2005; *Bower et al*., 2002; *Søiland et al*., 2008]. As we will see later, the question of transport across the Ridge is still an open question.

A more recent and very comprehensive study by *Sarafanov et al*. [2012] shows how altimetry and hydrography can work together to estimate transports in the northeast Atlantic. They combine seven summertime

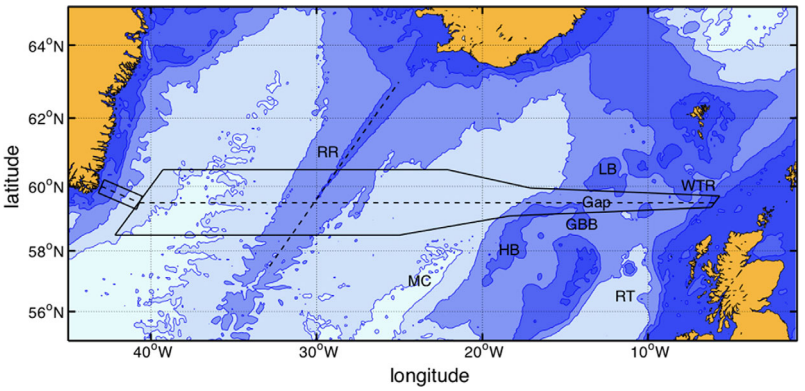

Figure 1. Bathymetric chart of the northeast Atlantic Ocean with Greenland in the west, Iceland in the center, and Scotland in the east. The bathymetric features referred to in this study include the Reykjanes Ridge (RR), Maury Channel (MC), Hatton Bank (HB), the Gap between George Bligh (GBB) and Lousy Bank (LB), Rockall Trough (RT), and Wyville-Thompson Ridge (WTR) to its north. The dashed line indicates the working section in this study. All data within the zonal domain will be moved to 59.5°N parallel to the RR. Similarly, all data used in the small box off Greenland will be moved to the dashed line parallel to the continental slope. Bathymetric contours at 200, 1000, 2000, and 3000 m.

hydrographic sections between Cape Farewell and Scotland with weekly AVISO maps of sea surface height to estimate the zonal and vertical distributions of meridional transport across the section. They define three layers separated by two isopycnals (27.55 and 27.8 kg m^{-3}): an upper ocean poleward flow, an intermediate layer, and a deep return flow layer west and east of the Ridge. These layers are subdivided zonally to look at transport in subsections in the Irminger Sea and Iceland Basin. A key finding of the study is that they estimate the MOC to be 16.6 $\pm$ 1.1 Sv (1 Sv = 10^6 m^3 s^{-1}) at 59.5°N.

In this paper, we are also interested in poleward flow at 59.5°N, but instead of altimetry to reference geostrophic velocity we use directly measured currents from the container freighter Nuka Arctica during her transits between Cape Farewell and Scotland; Figure 1 shows the location of the section along 59.5°N with a short angled extension in toward the southeast Greenland slope. We will use these velocity data in combination with upper ocean thermal and hydrographic data to attempt a more accurate estimate of poleward volume, heat, and freshwater flux. This is motivated by the few and rather large scatter of past heat flux estimates [see *Trenberth and Fasullo*, 2008, and references therein]. While we lack concurrent measurements of temperature and salinity, we can employ Argo profiles available in the vicinity of the vessel route from throughout the year to extend geostrophically the velocity field to 1900 m. Having data from throughout the year enables us to assess possible seasonal variations in transport. Lastly, thanks to two ADCP data sets of comparable scope and quality 13 years apart, we can estimate differences in volume transport between these periods, which might give us some insight into decadal changes. Thus, the novel aspect to this study is that we have detailed information on the upper ocean Eulerian velocity, temperature, and salinity fields. This should permit us to make an accurate estimate of the annual mean MOC and poleward heat and freshwater fluxes. A limiting aspect of this study is that we can only determine the upper ocean component of these fluxes, and must rely on the zero mass flux constraint and historical data at depth to complete the heat and freshwater flux calculations.

The velocity data come from an acoustic Doppler current profiler (ADCP) that has been in operation since late 2012 on the Nuka Arctica. It profiles currents underneath the vessel to as much as 800 m depth in good weather conditions. An earlier ADCP operation between 1999 and 2002 profiled currents to 400 m depth [*Knutsen et al*., 2005; *Chafik et al*., 2014; *Childers et al*., 2015]. The seasonal and long-term variability of the thermal field along the section have been monitored continuously since late 2000. Four times per year expendable bathythermograph (XBT) profiles are taken with an average separation of roughly 40 km between Cape Farewell and Scotland. These are useful to identify space-time variations in the upper ocean temperature field. Argo profiles of temperature and salinity in the vicinity of the Nuka Arctica route will be used to determine geostrophic shear to extend the directly measured velocity field to 1900 m depth. This permits us to include upper ocean poleward flow everywhere between Greenland and Scotland. Finally, we use WOA mean hydrography to extend the velocity profiles to the ocean bottom.

This paper is structured as follows: Section 2 will briefly describe the data sets and how they will be used here. Section 3 will construct the integrals of volume, heat, and salt transport. Section 4 will discuss the results and compare them with past estimates. Section 5 summarizes the principal findings of the study.

2. Data and Methods

The three data sets used here are the vessel-mounted ADCP velocity data, the XBT temperature profiles, and Argo profiles from the vicinity of the mean Nuka Arctica route, all within a zonal band centered at 59.5°N. Due to the extensive topography (the Wyville-Thompson Ridge, in particular) near Scotland this band is tapered to a narrow zonal wedge at the eastern end of the section. Following *Knutsen et al*. [2005] and *Chafik et al*. [2014], all profiles (ADCP, XBT, Argo) are relocated to 59.5°N along a line parallel to the Ridge on the grounds that the major axis of the Irminger Sea and Iceland Basins largely follows the same orientation. In short, the analyses in this paper will be performed as if all data had been collected along 59.5°N, what we will hereafter call the section. The section spans three major subdomains, the Irminger Sea, the Iceland Basin, and the Rockall Trough. These are separated by the Ridge and the George Bligh—Lousy Bank Gap (hereafter known as the Gap, see Figure 1), respectively. The Gap is shallower than the surrounding basins with its saddle point at 1000 m between the 1600 m deep Rockall Trough and 2000 m deep Iceland Basin. About 150 km east of Greenland, the zonal section is reoriented normal to the Greenland slope. All ADCP data within $\pm$25 km of this line are projected onto this line normal to the slope. Given that there are quite a lot of data we kept this band narrow to avoid influence of along-slope variations.

2.1. The ADCP Data

The ADCP instrument profiles currents underneath the ship by measuring the Doppler shift of short acoustic pulses transmitted down in four oblique directions. The Doppler shift of the backscattered signal as a function of time gives us a vertical profile of velocity relative to the ship along each of the four beams. The ADCP electronics rotates or remaps these "along-beam" velocities as a function of depth into two horizontal and vertical components relative to the instrument. To render the shipboard data useful from a scientific point of view, the ship's motion must be accounted for in order to produce geo-referenced velocity profiles. For fast-moving commercial vessels, the crucial information needed is heading of the ship. Speed is of course essential as well, but since it is usually the cross-track velocity that is sought, it is imperative that heading be known accurately. This is possible thanks to GPS-based compasses such as the Thales ADU-5, which gives instantaneous heading accuracy at the 0.05° level. Averaging heading as we do velocity over 3 min intervals leads to uncertainties that are substantially smaller. In Appendix A, we show that heading error is of less importance to the estimation of transport than uncertainties associated with the eddy velocity field (Appendix A). As in *Chafik et al*. [2014], all velocity data have been detided by computing the spatial dependence of the principal tidal components (M2, S2, N2, K1, and L2) in the upper 100 m using a least square method [*Dunn*, 2002; *Wang et al*., 2004]. Two ADCP data sets have been prepared for this study: the 150 kHz data set that reaches to 400 m depth (used in the *Chafik et al*. [2014] study), and the new 75 kHz data set that reaches to $>$700 m depth from late 2012 to February 2016. While both data sets have excellent quality, the latter set will serve as our primary data set thanks to its greater vertical range. For this study, all data have been binned into 10 km segments from southeast Greenland to the Scotland slope. We note again that all velocity and hydrographic profiles within a narrow band bracketing 59.5°N are projected onto this latitude in a direction parallel to the Ridge (see *Chafik et al*. [2014] for further details).

2.2. The XBT Data

XBT profiles are taken quarterly along the Nuka Arctica route to nominally 900 m with an average separation of 40 km, but these can vary considerably depending upon vessel speed and weather; in heavy weather the losses can be quite severe. In addition, the ship will sometimes deviate from its normal route to avoid severe weather conditions. These problems notwithstanding, over 1000 more or less uniformly distributed XBTs within $\pm$1° latitude of 59.5°N allow us to construct the mean temperature field, its seasonal cycle, and multiyear variability quite well, but we limit ourselves to the two periods for which we have ADCP data. We deseason the XBT data by first picking profiles in three areas: the central Irminger Sea, the central Iceland Basin (central regions in order to minimize influence from possible boundary current gradients), and the northern Rockall Trough. We treat the profiles in each of these groups as belonging to a

homogeneous data set (in space), but taken irregularly in time. A least square fit of a mean and annual sine/cosine function as a function of depth is then applied to each group. While the annual cycle fits differ in amplitude somewhat for the three regions for the purposes of this paper it will be quite adequate to average these into a single annual cycle as a function of depth, which is used to deseason all profiles. This gives us the 15 year mean temperature between Cape Farewell and Scotland. Subsets of the data can be used to examine variations between years. The temperature and depth accuracy of the XBT are nominally 0.1°C and 2% of depth, respectively, both sufficient for the purposes of this study.

2.3. Argo Data

The Argo data used here, comprising nearly 1100 profiles, from roughly the same period, complement the XBT data very effectively by extending the profiles deeper and by providing salinity as well. In order to maintain resolution of the density field, the Argo profiles are projected onto 59.5°N in the same way as the ADCP and XBT data. Here the profiles are grouped into 20 km bins (somewhat wider than the ADCP data in order to increase the number of profiles in each). The accuracy of the adjusted data is ± 2 dbars, ± 0.002°C, and $< \pm 0.01$ practical salinity units (PSU), respectively [*Riser et al.*, 2008]. The Argo data are deseasoned exactly as the XBT data, and used to construct zonal sections of mean temperature, salinity, density, and potential vorticity $(f/\rho)\Delta\rho/\Delta z$. Plotting these properties along isopycnals helps to identify regions of contrast and homogenization. Argo profiles tend to be more common over the deeper basins and less so along the banks and the Ridge where rapid flow advects floats past these regions rather quickly. This is another way XBTs and Argo floats complement each other since the former are deployed along the vessel route. Unfortunately Argo coverage of the East Greenland Current is limited and almost nonexistent in the Rockall Trough.

The Argo and XBT data are combined into a single "expanded XBT" data set to chart temporal variability of the upper ocean.

2.4. The Composite Data Set

This is the final step, to use the Argo mean density field to extend the velocity field to 1900 m depth. The approach taken here will be to use Argo density field to obtain the geostrophic velocity relative to an arbitrary zero velocity at the surface. We then remove this arbitrariness by lining up the geostrophic velocity to the measured velocity field. The profile data are collected into vertical bins of increasing thickness (10 m at the surface, 100 starting at 400 m, and 200 m below 1200 m) with the deepest vertical bin centered at 1900 m depth. These will later be resampled at equally spaced 16 m bins (that of the ADCP bin size) to facilitate the estimation of volume, heat, and salt fluxes.

Coupling Argo geostrophic velocity to ADCP velocity takes place in a set of steps: first to determine dynamic height anomaly (ΔD) from the surface down, second to determine vertical shear ($\partial v/\partial z$), and third velocity (v) relative to the surface:

$$\Delta D = \int_0^p \delta \, dp$$

$$\frac{\partial v}{\partial z} = -\frac{\partial \Delta D}{\partial x}$$

$$v = \int_0^z \frac{\partial v}{\partial z} dz$$

where δ is the specific volume anomaly and p is the hydrostatic pressure. ΔD, δ, and v are the functions of depth and location along the zonal section. The geostrophic velocity profile to 1900 m depth is then resampled onto the ADCP grid for the final compositing with the ADCP data by adjusting the geostrophic velocity to match the measured velocity at each 10 km point at 700 m depth. We now have velocity, temperature, and salinity to 1900 m depth. Integrals of mass (volume), heat, and salt flux follow directly from the above.

The limits of integration in the vertical can be in either depth (z) or density (σ) coordinates, but we will work primarily with the latter to better resolve the MOC aspects of poleward flow.

3. Observations

The approach we take here will be to present the mean hydrographic state and velocity fields separately first. We then use the mean density field to extend geostrophically velocity field to 1900 m to estimate poleward fluxes across the section. We thereafter use the WOA13 [*Locarnini et al*., 2013; *Zweng et al*., 2013] to extend to velocity field to the bottom as a consistency check. Lastly, we use the differences between the earlier and more recent ADCP data to estimate possible decadal variations.

3.1. The Hydrographic Picture

The two plots in Figure 2 show the deseasoned mean temperature and salinity fields between Greenland and Scotland using all Argo profiles with two sigma-theta (density) lines superimposed. The left plot shows clearly the shoaling of the temperature field from the Scotland slope to the Irminger Sea before it dips toward the East Greenland slope. The same overall pattern applies to density as well: sharp transitions take place at the Gap and across the Ridge. Even though the 100 km Gap might be viewed as wide, the underlying topographic ridge clearly acts as a dynamical barrier between the warm and saline Rockall Trough water and the somewhat cooler and fresher Iceland Basin water dominated by the flow north from the North Atlantic Current [*Bower et al*., 2002; *Lavender et al*., 2005]. Salinity, which serves more as a tracer, further emphasizes the transitions at the Gap and the Ridge indicating a measure of isolation of the water masses to either sides. At roughly 200–400 m depth over the eastern side of the Ridge (between ~30°W and 27°W) both temperature and salinity are weakly stratified [*de Boisséson et al*., 2012] below which both temperature and salinity reverse slope in such a way that the density field is all but level in this region. Right over the Ridge both isotherms and isohalines dip conspicuously down toward the ridge crest, but they do so in a density-compensated way such that the sigma-theta contours are nearly unaffected [cf. *Sarafanov et al*., 2012; *Mercier et al*., 2015]. While coverage near Greenland is limited to 34 Argo profiles, it is still enough to show both the reverse slope of the temperature field across the East Greenland Current and the core of high salinity water from the Irminger Current.

The annually averaged isopycnal perspective highlights the topographic influence of the Ridge (30°W) and the Gap upon the overlying density layers (Figure 3). The temperature field shows a major increase across the Irminger Current at 31–32°W and a lesser increase at the Gap (14–15°W). Salinity also exhibits a transition across the Ridge and the Gap. Potential vorticity (PV) increases from west to east across the Ridge showing a pycnocline centered at about $\sigma_\theta = 27.55$ kg m^{-3}. The density surfaces deepen and there is a further increase in the PV maximum at depth. Another striking feature is the salinity maximum between Scotland and the Ridge that hovers just below the surface. *McCartney and Mauritzen* [2001] argue that this

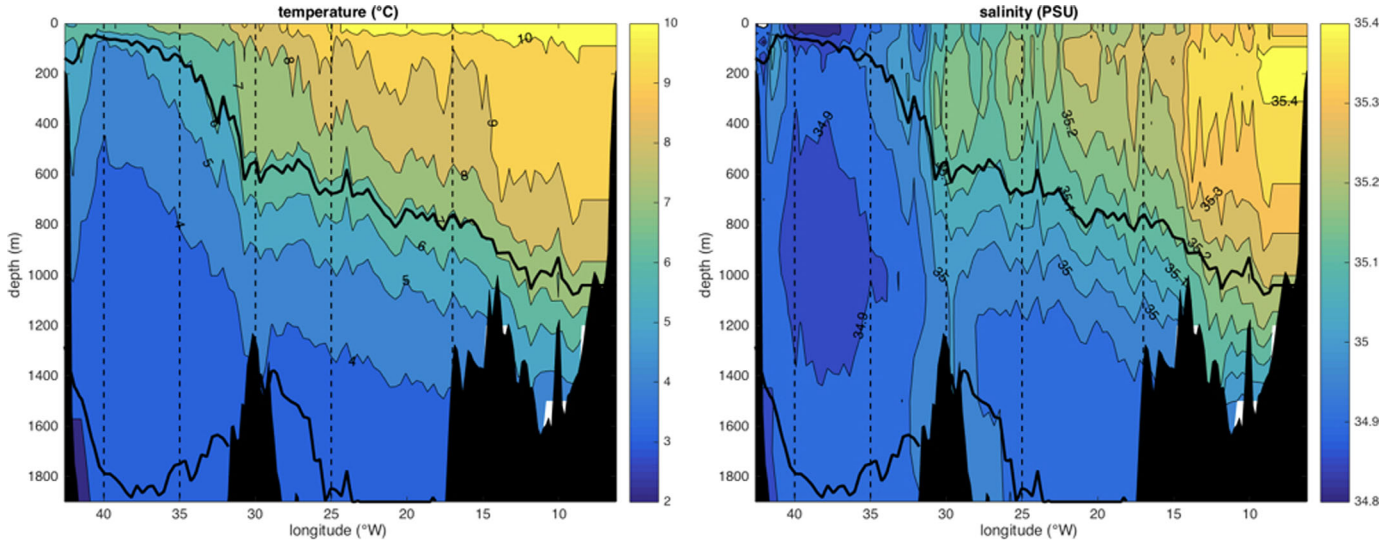

Figure 2. These two plots show the (left) deseasoned mean temperature field and (right) salinity field between the Greenland and Scotland shelf breaks using all ~1100 Argo profiles near 59.5°N in 20 km bins (~10 profiles/bin with 34 profiles in the EGC). No smoothing has been applied. The two heavy lines represent $\sigma_\theta = 27.55$ and 27.80 kg m^{-3}. The dashed lines separate the six subdomains used in the tables.

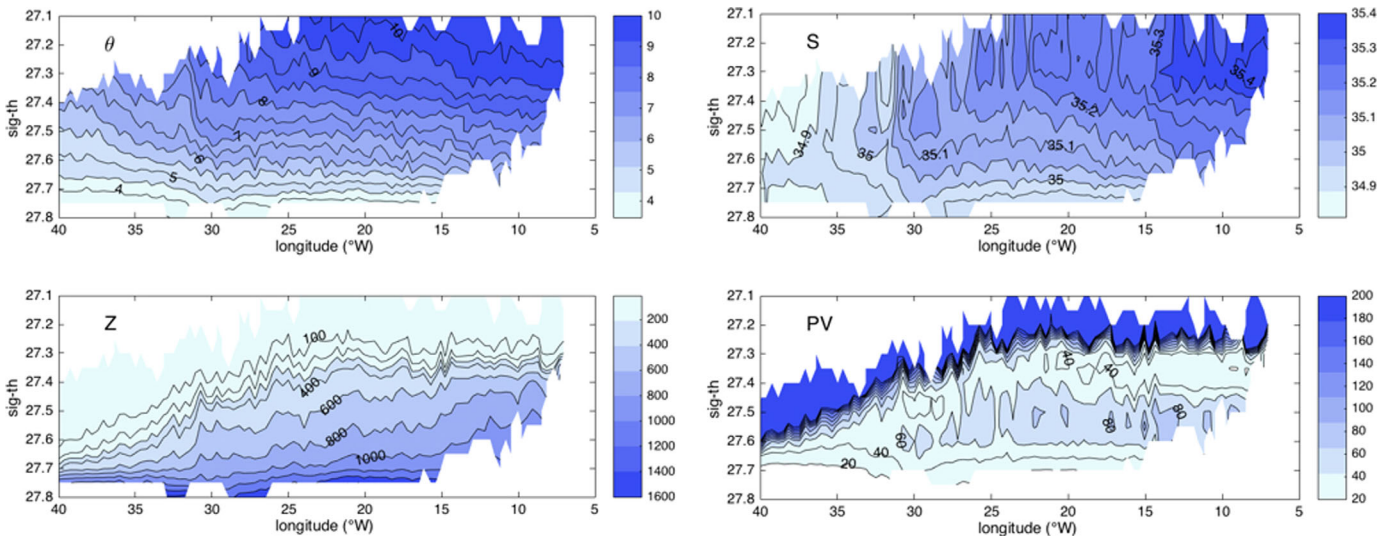

Figure 3. The four plots show from left to right, top to bottom temperature, salinity, depth, and potential vorticity (in units of 10^{-12}) as a function of σ_θ.

reflects the convective transfer of salt from the more saline surface waters in winter to the density surface that barely outcrops. Consistent with this, the rather sharp deepening of the salinity maximum and PV minimum to the 27.5 kg m^{-3} surface between ~26 and 28°W corresponds to the transition between the northward flow at and east of ~26°W, and the southward flow on the eastern side of the Ridge reflecting the longer, cyclonic pathway of NAC water north and around the Iceland Basin and hence exposure to the atmosphere before flowing back south along the RR.

The XBT data set gives the same overall picture as Argo for the upper ocean, but its higher resolution over the Ridge reveals further detail. In Figure 4, using both XBT and Argo data, the top plot shows the sharp rise in the isotherms to the west, both right over the Ridge at 31°W and also at ~33°W in the upper layers, both of which show increased thermal variance (not shown). These two rises may correspond to the two fronts in the Irminger Current noted by *Knutsen et al.* [2005]. The thermostad at 200–400 m east of the ridge crest shows up below which the isotherms level out. The bottom plot shows a clear reduction in mean temperature between 2001 and 2007.5 and 2007.5 and 2015 in the top 800 m in both the Irminger Sea and Iceland Basin, but not in the Rockall Trough [cf. *Robson et al.*, 2016].

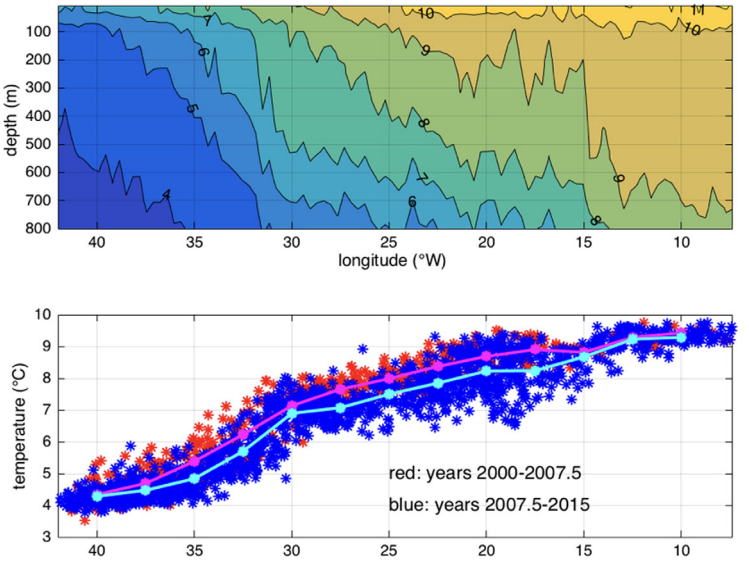

Figure 4. (top) Deseasoned mean temperature along 59.5°N from all XBT and Argo data. (bottom) Change in average temperature in the top 800 m between two observing periods using the same XBT and Argo data set. Due to the large number of data points (~2000 in all) the standard errors are as small as the dots so they are not plotted.

3.2. The Velocity Field

The Nuka Arctica operates on a 3 week schedule along a great circle path toward Cape Farewell and along a constant latitude eastbound. This eastbound transit will define our 59.5°N working section, but the great circle route, which approaches Cape Farewell from the northeast, enables us to construct a section normal to the East Greenland Current. Figure 5 summarizes the velocity database from these combined data sets.

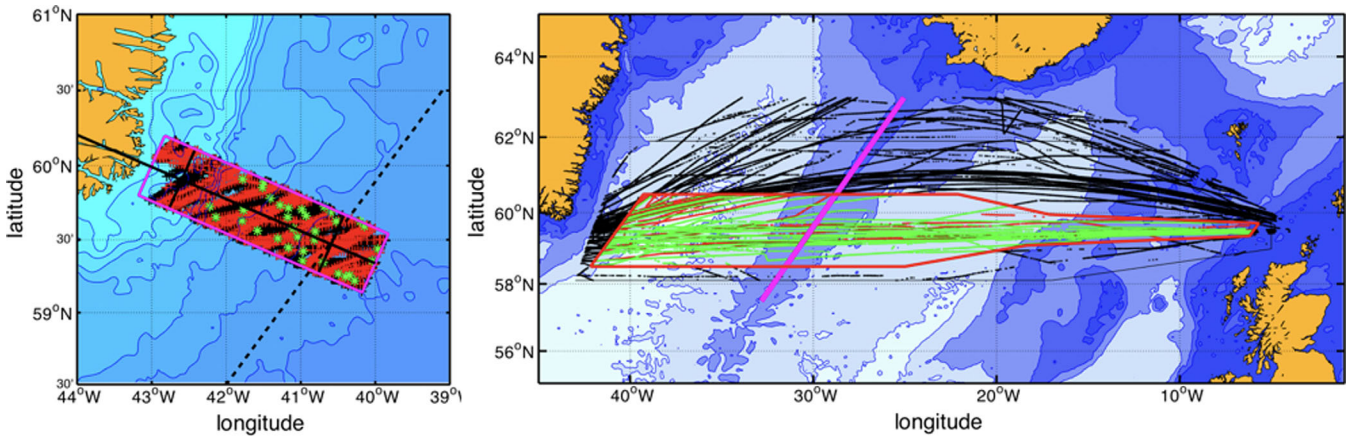

Figure 5. (left) Location of all ADCP data used to construct the mean flow in the East Greenland Current (red = earlier 150 kHz data; black = recent 75 kHz data). The green stars indicate Argo profiles. (right) Tracks of all 75 kHz data inside the zonal red box used to determine mean flow between the East Greenland Current and the Scotland Slope. Green and black dots are from eastbound and westbound transits, respectively. The magenta line indicates the Reykjanes Ridge axis. The East Greenland Current section (left plot) is drawn normal to the continental slope out to where it meets the zonal section at 59.5°N, 40.6°W. Its width is ±25 km.

The left panel shows where ADCP data have been obtained in the East Greenland Current, and the right panel shows the data from along the full zonal band. It is bound by 58.5°N to the south and 60.5°N to the north tapering to the east to exclude great circle transits near the Scotland slope so that all transits used here pass south of the Wyville-Thompson Ridge (Figure 1). This is an important geographical constraint we impose due to the ridge's impact on flow toward and along the Scotland slope [*McCartney and Mauritzen*, 2001; *Sherwin et al*., 2006; *Childers et al*., 2015]. The section across the East Greenland Current uses all ADCP profiles within 25 km to either side. These are further grouped into 10 km bins along the entire section. Figure 6 shows the integral of mean velocity normal to the section in the top 400 m between Greenland and Scotland. The integration is from west to east relative to the Ridge. The red and black curves apply to the 1999–2002 and 2012–2016 data sets, respectively. Both data sets are comparable in size; the latter has 78 ± 15 profiles per 10 km bin increasing sharply to more than twice as many west of 36°W. The two integrals track each other rather closely. The cyclonic circulation of the Irminger Sea shows up clearly with the high transport south in the East Greenland Current and north in the Irminger Current [*Våge et al*., 2011]. Both periods show a small net southward transport west of the Ridge, slightly stronger for the latter period. East of the Ridge across its slope and the Iceland Basin to 15°W the two integrals are almost identical at 4.65 Sv even though the eddy field causes the two integrals to cross each other several times. The Scotland Slope Current is all but the same for the two periods as well. However, the end points of the red and black integrals in Figure 6 indicate that between the two periods the net transport has increased to the south by 1.9 Sv (−0.5 to −2.4) west of the Ridge while to its east transport has decreased to the north by 1.3 Sv (8.2 to 6.9) for a total drop in the top 400 m of about 3.2 Sv. The large and partially overlapping error bars suggest caution of reading in too much in these patterns, but we will

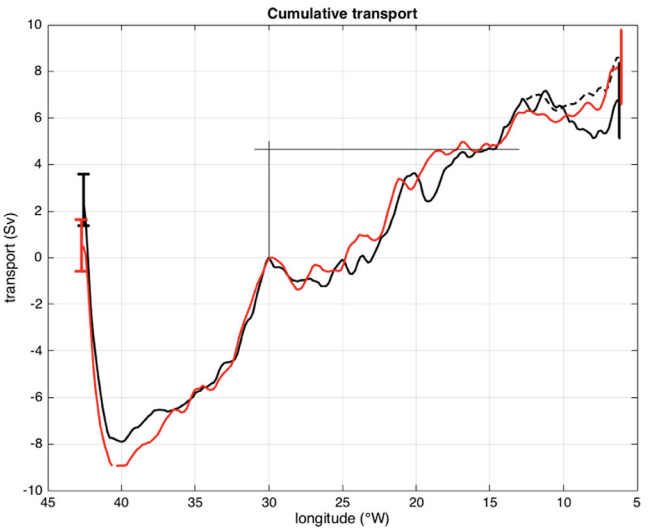

Figure 6. Integrals of transport in the top 400 m with respect to the Ridge (30°W). Red = earlier 150 kHz data; black = recent 75 kHz data. The vertical line at 30°W emphasizes the same transport east of the ridge to Hatton Bank for both data sets. A positive slope means poleward flow and vice versa. The dashed line indicates the revised cumulative transport (see text). The integral uncertainty is ±1.1 Sv at Greenland and ±1.6 Sv at Scotland.

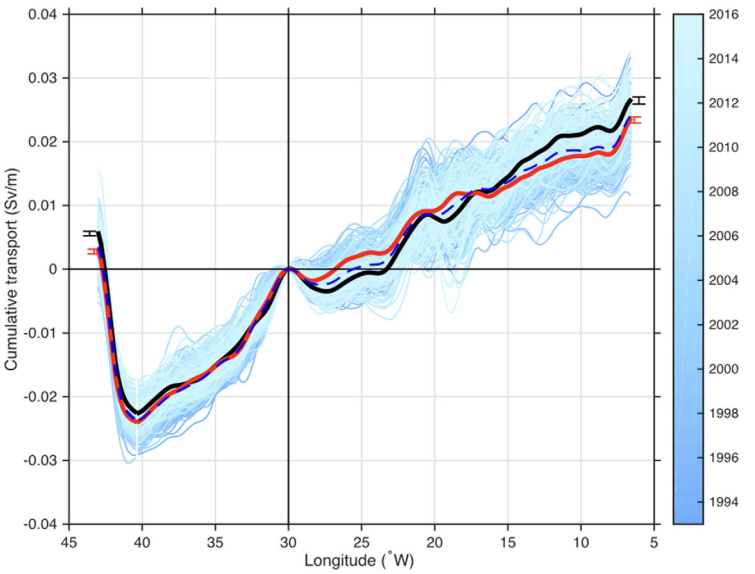

Figure 7. Integral of surface velocity relative to the Ridge at 30°W using the multisatellite sea surface heights provided by AVISO. The geostrophic surface velocity is estimated monthly in a 20 × 20 km grid inside the band from Greenland to Scotland and moved to the center line exactly as done with the ADCP data. The dashed blue line is the time-mean transport (1993–2015), while red/black thick lines are the 1999–2002/2012–2016 average transports, respectively. The thin lines plot individual monthly transport estimates between 1993 and 2015. The small standard error bars reflect the large number of sections for each period.

see later that they are mirrored in the altimetric record. A closer look at the integrals in Figure 6 shows that the integrals diverge in two specific areas: 38–37°W in the Irminger Sea and 11–8°W in the Rockall Trough. With respect to the Irminger Sea one might ask if this is related to the return of deep convection there in recent years [e.g., *de Jong and de Steur*, 2016; *Våge et al.*, 2009]. Between 14°W and 13°W the integrals show a clear ∼1.8 to 2 Sv increase, east of which the earlier record remains flat until the Slope Current is reached while the latter decreases to ∼5.2 Sv just west of the slope current. While the multiple crossings of the integrals between the Ridge and Hatton Bank reflect the finite number of samples available for averaging in an eddy-active region, the more gradual increase across the Iceland Basin suggests an eastward shift of the poleward flow there [*Häkkinen and Rhines*, 2009] (see also the eastward shift in the temperature field in Figure 4b). The striking anticyclonic variation at 20°W in the latter period is all but certainly associated with the PRIME eddy [*Martin et al.*, 1998; *Wade and Heywood*, 2001; *Chafik et al.*, 2014]. The virtually identical transports in all boundary currents and across the Iceland Basin for the two periods 13 years apart suggests that (i) the methodology of measuring currents over great distances can be done with considerable accuracy, O(1) Sv over 10^3 km [cf. *Worst et al.*, 2014]. This is further corroborated from altimetry along the same route. Figure 7 shows integrated surface transport based on monthly averages of AVISO SSH relative to the Ridge, exactly as in Figure 6. It replicates the stability of all boundary currents including the flow in the Iceland Basin. It picks up the anticyclonic activity associated with the PRIME eddy. It also shows the increased flow to the south between Greenland and the Ridge and even includes the divergence in transport in the Irminger Sea at 38–37°W seen in the ADCP record. Figure 7 also suggests a slight increase in the upper ocean circulation: stronger flow to the north east of the Ridge and stronger flow south to its west. Although speculative, this might be related to the more positive state of the North Atlantic Oscillation in recent years (http://www.cpc.noaa.gov/products/precip/CWlink/pna/nao.shtml). But returning to Figure 6, altimetry does not give any hint of the large drop in the Rockall Trough. Why such a striking difference in only this spot? We cannot prove it, but the difference may be due to the fact that while both data sets are comparable in volume (close to 20 transects) the earlier data have a more uniform meridional distribution throughout the zonal band whereas the latter transects follow a tighter track over the northern slope of Rosemary Bank. The sharp topography of the Bank may possibly be inducing a southward component of flow to its east. Whether or not this is the reason, the fact is that the earlier ADCP data set does not show this, and the cumulative altimetric integral east of ∼12°W is almost identical for both periods. In view of this, and the fact that altimetry has far more degrees of freedom, we will use the 1999–2002 data set between 12.5°W and 8°W to construct the full velocity field in this segment across the Rockall Trough. That the adjusted transport field (dashed line) does not track the 150 kHz data perfectly (red line) in Figure 6 is due to interpolation from different sampling intervals both horizontally and vertically. The differences are considered small compared to the overall uncertainties. The estimation of the integral uncertainty is discussed in Appendix A1.

To summarize: the ADCP and altimetric record both show an increased flow to the south west of the Ridge, whereas to its east the altimetric record points a comparable increase in northward surface transport.

3.3. Combining Hydrography and Velocity

Here we use the Argo data to geostrophically extend the directly measured mean velocity to 1900 m depth. In order to retain as much of the directly measured velocity profile as possible since it is both accurate and detailed (resolves the boundary currents), the transition to the geostrophic extension is done at 700 m with the exception of the 12.5–8°W segment where the extension starts at 400 m (the maximum reach of the earlier ADCP data set). The velocity data are generally of high quality, but the volume of data (i.e., degrees of freedom) decreases rapidly beyond this depth. The lower resolution, smoother geostrophic velocity field was resampled to the ADCP grid after which an offset to the geostrophic profile is added so that velocity is continuous from the ADCP to the geostrophic profile. The resulting field is shown in Figure 8. It is important to note that this stitching will impose the ADCP variability on the underlying geostrophic field although some additional structure at depth may result from the wiggles inherent in the density field. All the boundary currents, the East Greenland Current, the flows north and south along the Ridge and the Slope Current, albeit narrow, can be seen clearly. The PRIME anticyclonic eddy activity shows up around 20°W in the Iceland Basin [*Chafik et al*., 2014, see their Figure 5]. Superimposed on the velocity field are the deseasoned σ_θ lines, shallow in the cold Irminger Sea and deepening to the east across the Irminger Current and Iceland Basin. Two of these, $\sigma_\theta = 27.55$ and 27.80 kg m^{-3}, are highlighted. The dashed vertical lines separate the East Greenland Current, the Irminger Sea, the Irminger Current, the eastern Ridge region, the Iceland Basin, and the Rockall Trough domains. (These are labeled EGC, IS, IC, ERR, IB, and RT in the tables below.) These and the isopycnals are chosen to define subregions that correspond to the subdivisions used in the *Sarafanov et al*. [2012] paper.

The first step is to determine the total volume transport across the section from the surface down as a function of both depth and density. To do this we extend the velocity below the reach of the Argo array to the bottom by referencing or aligning the geostrophic shear estimated from WOA13 to the computed velocity at 1900 m depth. The resulting transport integrals are shown in Figure 9. The maximum flow to the north in the left plot is about 11.0 Sv at ~900 m depth (black curve) while in density coordinates (right plot) the maximum reaches 18.4 Sv at $\sigma_\theta = 27.55$ kg m^{-3}, the shallower of the two highlighted isopycnals in Figure 8. The reason these two maxima differ so much is that the northward flow east of the Ridge (red curve) is counteracted by a strong southward flow west of the Ridge in the East Greenland Current (green curve). This extreme asymmetry was evident in Figures 6 and 7 as well. In density space, the 27.55 σ_θ contour reaches almost to the surface in the Irminger Sea so the top layer is overwhelmingly dominated by poleward flow in the Irminger Sea, the Irminger Current, and the Iceland Basin. As we will see shortly, this emphasizes the vertical or overturning mode of the MOC: almost everywhere the top layer flows north with all return flow in the two lower layers in the East Greenland Current.

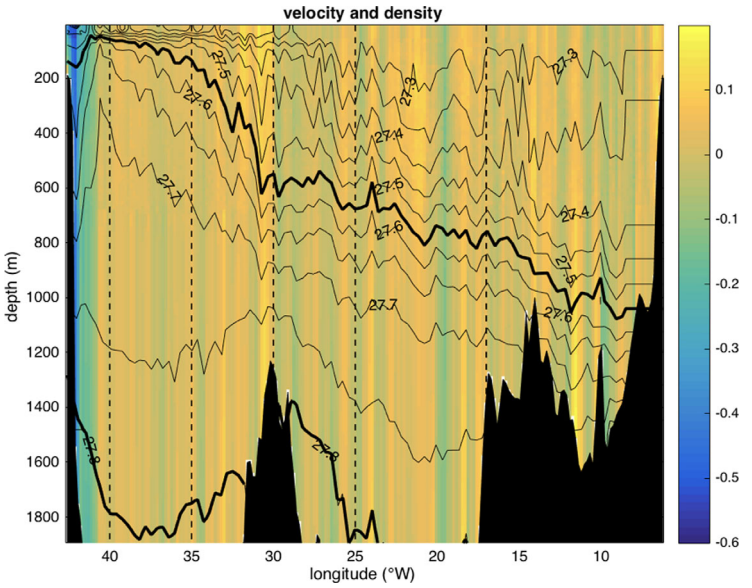

Figure 8. Zonal-vertical view of poleward velocity constructed from the ADCP data to 700 m and Argo hydrography to 1900 m. The dashed lines separate the six subdomains EGC, IS, IB, ERR, IB, and the RT in Tables 1, 2, and 3. Two σ_θ lines 27.55 and 27.80 kg m^{-3} separate the top, middle, and bottom layers. Not shown is the extension to the bottom.

A straight line fit to the total transport curve (Figure 9) between 200 and 100 m depth representing a geostrophic shear and extrapolated to the surface leads to an approximately negative −1.2 Sv, a deviation which we interpret as the annual-mean Ekman transport to the south. This compares well to −0.9 Sv using the annual average wind stress obtained

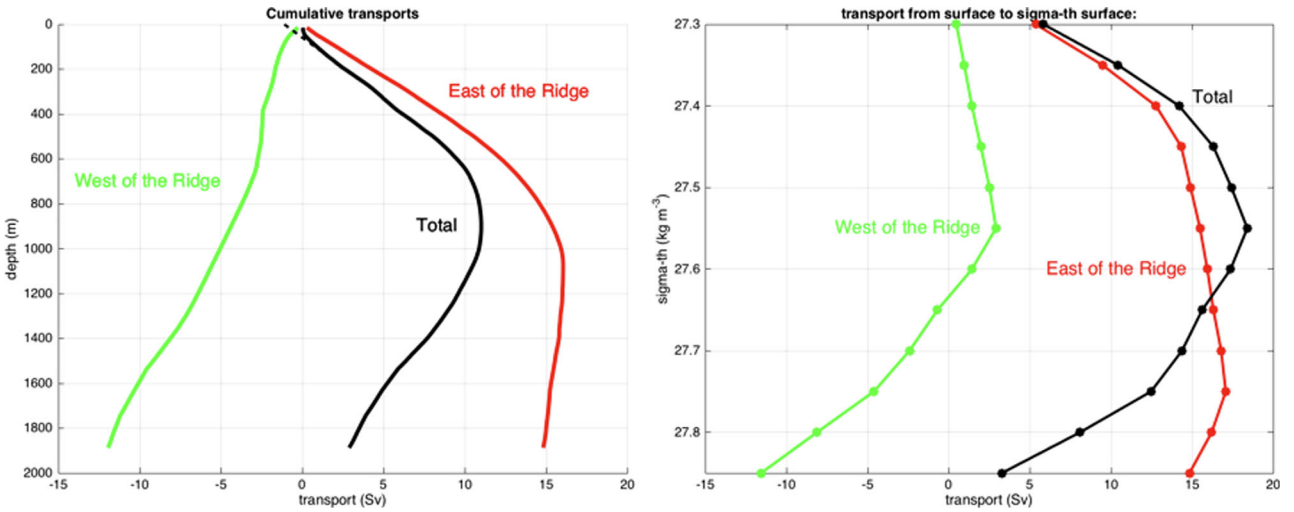

Figure 9. Integrals of poleward transport from the surface down west (green) and east of the Ridge (red) as a function of (left plot) depth and (right plot) σ_θ. The difference between the black line and the dashed extension to the surface in the left plot represents the Ekman layer contribution (see text).

from NCEP [*Kalnay et al.*, 1996], and −1.3 Sv using a corresponding average wind stress from ERA [*Dee et al.*, 2011].

The next step is to estimate partial transports of volume, heat, and salt for each of these 18 cells, 3 in the vertical by 6 in the horizontal (Table 1). The columns represent the six domains between Greenland and Scotland defined earlier while the rows represent the three layers, surface to 27.55, 27.55 to 27.80 (or 1900 m), and 27.80 (or 1900 m) to the bottom. The 1900 m limit is used where the 27.8 surface is deeper than this; fortunately the difference is small [cf. *Sarafanov et al.*, 2012]. Appendix A discusses in detail the procedure for estimating flux uncertainties.

The right column shows the layer sums. Figure 9 indicates that the MOC reaches a maximum at the $\sigma_\theta = 27.55$ surface. Subtracting the middle layer transport from the top layer tells us that the bottom layer transport should = −8.54 Sv to provide MOC closure. This is −2.67 Sv stronger than we had estimated from the geostrophic extension to the bottom layer and is larger than we would have liked, but given the two-stitch construction (ADCP-to-Argo-to-the smoother WOA13) of the top-to-bottom velocity field perhaps we should not be surprised. As we will see in section 4, there is reason to think our original deep flow estimate in the EGC (−4.79 Sv) is too low. We therefore add the −2.67 Sv to the deep EGC cell to obtain −7.46 Sv; this balances the flow north and south. We take this step not to estimate the strength of the MOC, this we now know from the ADCP and Argo data, but to estimate heat and freshwater fluxes.

Next, by integrating the local product of velocity and temperature we can estimate the corresponding temperature transport for each cell (Table 2).

The sum of these partial fluxes equals 399 TW. While the uncertainty in each cell is set by the corresponding flux uncertainty, the uncertainty of the net heat flux is governed by the uncertainty of the MOC: ±3.4/18.4 × 399 = 74 TW because the temperature field is essentially constant. Another way to put this is to note that 399 TW divided by 18.4 Sv implies a mean temperature difference of 5.4°C. The heat flux variations result principally from variations in the MOC, not the temperature field.

Table 1. Partial Volume Fluxes in Sv at 59.5°N[a]

Layer	EGC	IS	IC	ERR	IB	RT	Sum
<27.55	−3.36 (0.12)	0.39 (0.18)	5.89 (0.73)	−0.1 (1.10)	7.18 (1.60)	8.41 (2.69)	18.41 (3.4)
27.55–27.80	−23.54 (1.80)	5.11 (3.14)	7.87 (2.40)	−2.50 (1.66)	3.92 (2.77)	−0.73 (1.36)	−9.87 (5.5)
>27.80	**−7.46** (0.72)	−0.13 (2.03)	0.9 (0.55)	−2.04 (0.92)	0.19[b] (0.92)	–	**−8.54** (2.6)

[a]The top row for each layer represents the estimated mean flow; the numbers in parentheses represent the uncertainties.
[b]Section IB in the bottom layer between 21°W and 25°W. The numbers in bold are chosen to close the MOC budget.

Table 2. Partial Temperature Transports in TW at 59.5°N

Layer	EGC	IS	IC	ERR	IB	RT	Sum
<27.55	−80	10	170	2	248	311	661
27.55–27.80	−411	84	147	−46	75	−12	−163
>27.80	−89	1	12	−26	3[a]	–	−99

[a]Section IB in the bottom layer between 21°W and 25°W. To keep the table simple, the error estimates are not shown, but they scale according to transport uncertainties (Table 1); roughly 15–30% for the major components.

We return to this in section 4.

Next, we apply the same approach of integrating the product of velocity and salinity to obtain partial salt flux for each cell (Table 3).

The sum of all these partial fluxes = 0.069 × 10^8 kg s^{-1} positive to the north. This is the net salt flux north for an 18.4 Sv MOC with zero net volume transport and reflects that fact that the surface waters are saltier. The corresponding freshwater flux can be estimated given zero net salt transport, which can be done either by reducing the flow north in the top layer (the RT cell, say) or increasing the flow south in the bottom EGC cell, say). Either way the departure from zero volume flux will represent the required freshwater transport to balance the difference between the warm salty upper and cold fresh lower layers. Reducing the top layer flow by 0.0690/6.492 × 18.4 Sv = −0.196 Sv. Increasing the bottom layer flow to the south by 0.0690/2.98 × 8.54 = −0.198 Sv (the − sign means to the south). The small difference reflects the fact that salinity itself has a tight range between 34.95 and 35.35 PSU (Figure 2b). This can be demonstrated by considering that a mean salinity, 35.15 PSU, multiplied by an average −0.198 Sv gives us 0.070 × 10^8 kg s^{-1}, which is close to what we have above. Since the salinity field is quite well known, accuracy of the freshwater transport by the MOC is set principally by the uncertainties in estimating the MOC: 3.4/18.4 × 0.198 = 0.037 Sv. We return to this in the next section.

4. Discussion

Section 4.1 comments on the Rockall Trough correction and the role of topography. Section 4.2 discusses the uncertainties associated with all flux estimates. Section 4.3 discusses the MOC adjustment. Section 4.4 puts these flux estimates into a larger context of what has been reported in the literature.

4.1. Rockall Trough Correction

Had we not had the 2012–2016 data set, this problem would not have arisen since the 0–400 m integral of the earlier ADCP data (red curve in Figure 6) follows so closely the altimetric integrals (Figure 7). But the decision to use the latter ADCP data set was made early on because the data reach deeper and because the ADCP program is ongoing. There will soon be more data for a completely independent analysis. Whether or not our supposition that Rosemary Bank plays a role in the transport decrease across Rockall Trough remains to be seen. It is worth noting here that the spread of Nuka Arctica transects means that she samples the velocity field throughout the banks region. A study of how the local topography shapes the flow through the region including why the North Atlantic Current prefers to connect to the Scotland Slope Current north rather than south of the Wyville-Thompson Ridge [*Childers et al.*, 2015] could be quite interesting.

Table 3. Partial Salt Transports in Units of 10^8 kg s^{-1} at 59.5°N

Layer	EGC	IS	IC	ERR	IB	RT	Sum
<27.55	−1.174	0.135	2.066	−0.034	2.529	2.97	6.492
27.55–27.80	−8.222	1.783	2.754	−0.875	1.372	−0.255	−3.443
>27.80	−2.602	−0.046	0.315	−0.714	0.067[a]		−2.980

[a]Section IB in the bottom layer between 21°W and 25°W. To keep the table simple, the error estimates are not shown, but they scale according to transport uncertainties (Table 1); roughly 15–30% for the major components.

4.2. Flux Uncertainties

The procedure for estimating flux uncertainties is straightforward and based on velocity variance and degrees of freedom. Appendix A spells out the analysis of uncertainties for all partial volume transports in Table 1. The overall uncertainty of the MOC is ±3.4 Sv. While this is what the formal error assessment gives us, it may be on the conservative side because some fraction of the eddy variability—especially contributions by coherent features such as the PRIME eddy in the Maury Channel west of Hatton Bank—will cancel out in terms of cross-line fluxes. A comparison of Figures 6 and 7 also suggests that the uncertainty estimate may be on the conservative side because the 0–400 m integral mirrors the surface transport estimated from altimetry rather well. Indeed, Figure 7 indicates that the surface transport during the latter period is greater than the overall mean (dashed line) whereas the earlier period was close to the mean. This suggests that our 18.4 Sv MOC is probably on the high side with respect to a long-term mean.

The uncertainties for the temperature and salinity flux estimates are assumed to be dominated by the velocity field so the uncertainties in Tables 2 and 3 are governed by the fractional transport uncertainties from Table 1. The impact of the seasonal variations in temperature and salinity at the surface is rather minor: holding the velocity field constant, but using the late summer extrema for T and S, a maximum in temperature and a minimum in salinity, increase the heat and freshwater fluxes by 21 TW and 0.002 Sv, and vice versa in winter. While these variations are significant as such, they are minor compared to the overall uncertainty of the flux estimates. Perhaps more interesting might be the heat flux consequence of the 0.5°C cooler temperatures during the latter period in the Iceland Basin (Figure 4). Multiplying this by 7 Sv representing transport in the top layer (about 700 m thick) we obtain 4×10^6 (heat capacity) × 0.5°C × $7 \times 10^6 = 14$ TW. From a hydrographic point of view 0.5°C lower temperatures throughout the NE Atlantic is significant, but 14 TW is small compared to the uncertainty of the MOC heat flux. Clearly accurate knowledge of the velocity field is key to estimating fluxes.

4.3. The MOC Adjustment

The addition of 2.67 Sv in the Rockall Trough results in a mismatch between the upper and lower limb of the MOC as originally estimated. Because the upper limb is directly measured (ADCP to 700 m and Argo to $\sigma_\theta = 27.55$ kg m^{-3}), we think the 2.67 Sv mismatch is due to issues with the geostrophic extension to the bottom. In particular, the WOA13 is a smoothed product that may not adequately resolve the boundary currents. We mentioned earlier that the original estimate for transport in the deep EGC might have been too low, which is why we add this to the deep EGC cell to obtain −7.46 Sv there. This number is still on the low side, but close to other studies: *Sarafanov et al*. [2012] report −10.3 Sv, *Bacon and Saunders* [2010] report −9 ± 0.8 Sv, *Holliday et al*. [2009] obtain −12.3 Sv (a single, but high-quality section), *Våge et al*. [2011] obtain −9.6 ± 1.4 Sv (but suggest that only 2.4 ± 0.5 Sv comes from the Denmark St.), and *Mercier et al*. [2015] get about −8.1 Sv (with a 5–11 Sv range estimated from six sections in their Figure 3 using $\sigma_1 = 32.43$ as a proxy for $\sigma_\theta = 27.80$) at the OVIDE line. The dense water in the deep EGC comes from the Denmark St. and is diluted by entrainment of water of intermediate density. Several studies suggest about 4 Sv water denser than 27.8 kg m^{-3} [*Girton et al*., 2001; *Macrander et al*., 2005; *Dickson et al*., 2008] flowing through Denmark St. More recently *Jochumsen et al*. [2017] argue for 3.2 Sv as a long-term average with no trend. While there is some very dense water ($\sigma_\theta > 28.0$) in the Denmark St. [*Mastropole et al*., 2017], is its supply great enough to increase the flux of water with $\sigma_\theta > 27.8$ by a factor 3 (from 3.2 to O(10) Sv)? Given this wide range of estimates and uncertainties on the one hand yet highly localized flow south both near the surface and at depth, it seems like a strong case could be made for a sustained monitoring program with a moored current array at depth with the Nuka Arctica ADCP covering the upper ocean using XCTDs in addition to Argo to fill in the upper ocean density field. Almost all deep water of Nordic Seas origin in the MOC passes through here.

4.4. The Larger Context

The layout of our flux estimates followed that used by *Sarafanov et al*. [2012] study, which was based on the combination of seven high-resolution summertime hydrographic sections and satellite altimetry to provide a reference velocity. The lack of any (or very little) seasonal signal (Appendix A) makes a comparison between these two studies easier to consider. Our Table 1 corresponds to their Figure 8. The overall agreement is quite good: their MOC = 16.6 ± 1.1 versus our 18.4 ± 3.4 Sv. Good agreement can be seen in many of the subfluxes as well. East of the Ridge they report 15.5 Sv in the top layer versus our 15.9 Sv. An

important issue is that these are both large numbers given that only about 6.1 Sv continues into the Nordic Seas according to *Childers et al*. [2014], or 6.5 Sv, by combining 3.8 Sv in the Faroe Current [*Hansen et al*., 2015] and 2.7 Sv in the Faroe-Shetland Channel [*Berx et al*., 2013]. This leaves ∼9 Sv that must be exported in some combination across the Ridge north of 59.5°N or transferred diapycnally to the intermediate layer. *Childers et al*. [2015] suggest ∼1.5 Sv crossing the Ridge in the top 400 m based on a single hydrographic section along the ridge crest. Since crest depth north of 59.5°N is on average a bit more than twice as deep it is possible that the top-to-bottom cross-ridge flow is at least twice as large at 3 perhaps 4 Sv. Very likely there is a flow across the Ridge along the Iceland shelf break and leakages through fracture zones [*Bower et al*., 2002], but how large these might be remains to be determined. Upper-layer water is known to be entrained into the intermediate layer through entrainment by Iceland-Scotland Overflow Water [*Beaird et al*., 2013]. In addition, the $\sigma_\theta = 27.55$ surface layer can outcrop in wintertime even in the Iceland Basin allowing for conversion of upper layer water to densities >27.55 kg m^{-3}. The flows into the Nordic Seas are monitored rather closely so these are reasonably well known, but cross-Ridge and diapycnal fluxes are not. Quantifying these would be a big step in identifying fluid pathways from the top to the middle layer.

West of the Ridge the big difference between this and the Sarafanov et al. study is in the East Greenland Current. While the totals are virtually identical: 34.4 Sv (this study) versus 32.1 Sv (theirs) we find the bulk of the southward flow in the middle layer and only −7.46 Sv in the bottom layer compared to their −10.3 Sv, as discussed earlier. They also have a 2 Sv larger flow south in the top layer.

Our 18.4 ± 3.4 Sv estimate for the MOC (in density space) is not as tight as we had hoped for, but a couple of points can be made. First, the principal flows in Figure 6 are strikingly similar for the two periods. Except for a difference at the Greenland shelf break (not shown) the EGC transport is virtually the same for both periods. The same applies to the Irminger Current, the flow north in the Iceland Basin, and the Scotland Slope flow; all suggesting a tightness to the flow that is not reflected in the uncertainty estimate. Second, the altimetric record in Figure 7 suggests that the upper ocean circulation was stronger during this latter period during which time the surface transport integral east of the Ridge = 0.0265 versus the long-term mean of 0.0240 Sv m^{-1}. Multiplying the difference (0.0025 Sv m^{-1}) by 700 m (as a measure of the top layer thickness) implies a 1.75 Sv greater transport during this time suggesting a longer-term average might be ∼1.5 Sv less than our estimate. While Figure 7 also shows a stronger flow south west of the Ridge during this time (0.0056 – 0.0035 = 0.0021 Sv m^{-1} difference) the corresponding top layer transport increase to the south in the top layer (200 m thick, say) would only be ∼0.4 Sv suggesting that most of the decrease (∼1 Sv, say) is lost to lower layers. The 18.4 Sv MOC and 399 TW heat transport implies a 5.42°C average temperature difference between the upper and lower limb. Adjusting the MOC downward by 1 Sv implies a ∼22 TW reduction in heat transport suggesting a long-term mean of about 377 TW (with unchanged uncertainty). A corresponding long-term estimate for freshwater flux would be $-0.20(1 - 1/18.4) = -0.19 \pm 0.04$ Sv. It is assumed here that the altimetric variation applies to the top layer and that the return flow is in the bottom layer, but we do not really know this. If the return flow is in the intermediate layer the reductions in heat and freshwater transport will be less than estimated.

To summarize the above, the sample mean volume, heat, and freshwater fluxes are 18.4 ± 3.4 Sv, 399 ± 74 TW, and −0.20 ± 0.04 Sv. Using the 23 year altimetric signal as a guide for a longer-term mean, these numbers would be adjusted to about 17.4 Sv, 377 TW, and −0.19 Sv with unchanged uncertainties. Even though this adjustment is small in the sense that it is within the estimate uncertainties, it takes advantage of measured variations in sea level estimated along exactly the same route across the NE Atlantic. This adjustment also provides a measure of likely variations in heat and freshwater fluxes on decadal time scales due to changes in strength of the MOC.

Our estimate is not as tight as the 16.6 ± 1.1 *Sarafanov et al*. [2012] estimate, but it has been obtained from entirely different data sets (ADCP plus Argo) albeit with one important adjustment using altimetry. *Mercier et al*. [2015] estimate 16.9 ± 1.5 Sv for the MOC at the OVIDE line. They and *Sarafanov et al*. [2012] both depend upon mean dynamic topography, but use different hydrographic data sets. *Willis* [2010] estimates 15.5 ± 2.4 Sv at 41°N, which given the uncertainties is in line with the above estimates.

There are few direct estimates of heat and freshwater transport east of Greenland at these latitudes. The nearest one appears to be from the OVIDE line, which coincides with ours west of the Ridge, but turns SE toward Portugal instead of continuing straight east. *Mercier et al*. [2015] report 0.5 ± 0.06 PW from their

seven summertime sections. Given that their section lies mostly to the south of ours in a region of net heat loss to the atmosphere, it should be greater than our 399 ± 74 TW estimate. *Bacon* [1997] estimates 0.28 ± 0.06 PW and -0.17 ± 0.06 Sv heat and freshwater fluxes, resp. His section runs from Greenland to Ireland so it parallels our section more closely than the OVIDE line. Even closer to our line, *Dobroliubov* [1997, quoted in *Wijffels* [2001]] report -0.13 and -0.20 Sv freshwater fluxes at 58°N using 1980s and 1990s hydrographic data.

5. Summary

This study of the upper ocean velocity structure between Greenland and Scotland during two periods (1999–2002 and late 2012 to early 2106) suggests very similar poleward transports in the top 400 m, marginally stronger in the more recent period, and may be due to a somewhat higher NAO index during the latter period. This also argues against a slow-down of the MOC, the major constituent of this circulation, between these two periods. The principal flows, the East Greenland Current, the Irminger Current, the flow north in the Iceland Basin, and the Scotland Slope Current are nearly identical. Topography and inadequate sampling in the Rockall Trough led to one disagreement between the two periods that had to be resolved using altimetry. We used the latter ADCP data set for the analyses in this study thanks to its deeper reach, better temporal match to available Argo profiles, and the fact that the program is ongoing. By combining the annually averaged ADCP data with similarly averaged Argo profile data from along the same zonal section we have constructed the mean deseasoned velocity field normal to the section as well as the mean fields of temperature and salinity. These allow us to estimate the strength of the MOC in both density and depth coordinates as well as the net fluxes of heat and freshwater.

To facilitate comparison with the earlier *Sarafanov et al*. [2012] study along the same section, we take the same approach and find to within measurement uncertainty the same strength of the MOC: our 18.4 ± 3.4 Sv versus their 16.6 ± 1.1 Sv between the surface and $\sigma_\theta = 27.55$ kg m^{-3}, in both cases the density surface where the MOC integral reaches a maximum. Integration as a function of depth instead of density leads to a maximum of 11 Sv at ~850 m depth.

The agreement between this study and the *Sarafanov et al*. [2012] is noteworthy as they are obtained using quite different approaches. While both depend upon hydrography and geostrophy, our study uses direct measurement of currents for the upper ocean and a random array of Argo profiles whereas they use repeat hydrography and a mean dynamic topography. Theirs is a summertime estimate, ours is an annual average. Taken together these two studies provide testimony to the complementary contributions provided by ADCPs, which "scan" the upper ocean velocity structure in considerable detail from vessels in regular traffic, and altimetry, which "sees" only the surface, but does so at high sampling rates.

By integrating the products of mean velocity and temperature and salinity, respectively, we obtain total heat flux and freshwater flux subject to the constraints of zero net volume transport and salt transport. These results, 399 ± 74 TW and 0.20 ± 0.04 Sv, are to our knowledge to most accurate estimates to date, with the uncertainties principally due to variations in strength and position of the velocity field. It should be noted that all these fluxes are those associated with the MOC. This does not imply an absence of other flows, such as contributions across the Arctic from Bering St or flows along the Scotland shelf (both less than 1 Sv).

Finally, using the altimetric record along 59.5°N we suggest that our estimates for the 2012–2016 period may be somewhat on the high side with respect to the 23 year average. A more representative long-term average for the MOC, heat, and freshwater fluxes might be 17.4 Sv, 377 TW, and 0.19 Sv with unchanged uncertainty limits.

Appendix A: Estimating Flux Uncertainties

This section will be divided in two sections, the first part estimating the transport uncertainties in Figure 6 and the second part the uncertainties of the individual cells in Table 1. The uncertainties in Tables 2 and 3 will follow directly.

Table A1. Estimation of Transport Error for Each of the Boxes in Figure 8

Layer	EGC	IS	IC	ERR	IB	RT	Rms
v_u	0.14	0.14	0.14	0.14	0.14	0.14	
v_l	0.1	0.1	0.1	0.1	0.1	0.1	
L	120	280	280	280	450	620	
DoF	10	23	23	23	38	52	
H_{top}	100	100	400	600	700	1000	
H_{middle}	1500	1700	1300	900	1200	500	
H_{bottom}	600	1100	300	500	800		
<27.55	0.12	0.18	0.73	1.10	1.60	2.69	3.4
27.55–27.80	1.80	3.14	2.40	1.66	2.77	1.36	5.5
>27.80	0.72	2.03	0.55	0.92	0.92[a]		2.6

[a]Section IB in the bottom layer between 21°W and 25°W (225 km in length).
Note: The large uncertainties in the middle layer reflect its thickness in the IS and IB.

Estimating transport across long lines accurately from vessels in rapid motion depends crucially on the accuracy of vessel heading measurement and was addressed in the earlier study by *Chafik et al*. [2014]. Since then our experience with heading errors suggest that heading bias, unquestionably the most serious measurement uncertainty when estimating total transport across long lines, is less of an issue than previously thought. We base this statement on the fact that (i) upper ocean ADCP transport and sea level difference from altimetry are in close agreement and (ii) that the changes west and east of the Ridge between the earlier and latter observing periods are quite similar. This conclusion is based on the adjusted velocity field in Rockall Trough.

More specifically, the heading calibration is checked whenever and wherever the vessel is operating in shallow water operating what is called the bottom track mode. These corrections are typically a few hundredths of a degree. Averaged over all trips a residual uncertainty would be about 0.01°. At a vessel speed of 16 kt (8 m s^{-1}), this would result in a Greenland to Scotland surface layer transport (west and east of the Ridge) of 0.01° × (π/180°) × 8 m s^{-1} × (600 and 1400) km = 0.00084 and 0.0020 Sv/m, respectively. Multiply these by 400 m and assuming little vertical shear we obtain an upper ocean uncertainty of 0.33 and 0.78 Sv for the two subsections. Comparing these to the endpoint integrals in Figure 6 we see these are notably smaller than the uncertainties shown. We also note that upper ocean transport is greater for the latter period in both the ADCP and altimetric estimates lending further credence to the ADCP estimates. This is not to say there is no heading bias at all, merely that the principal uncertainty of the transport integrals is due to the limited degrees of freedom in reducing the impact of eddy variability, next paragraph.

Taking the same approach as in *Chafik et al*. [2014] the estimated transport uncertainty per unit depth is defined as v′ × length of section/$\sqrt{}$(DoF × N) where v′ (~0.14 m s^{-1}, discussed in next paragraph) is RMS velocity, DoF is degrees of freedom (distance divided by a correlation scale of 12 km), and N (~20) expresses the effective number of sections. It has the units m^2 s^{-1}, i.e., transport per unit depth. Inserting these values and multiplying by layer thickness, 400 m, gives us transport uncertainty, which equals ±1.6 and 1.1 Sv, east and west of the Ridge, respectively. These are indicated in Figure 6. When comparing Figure 6 to Figure 7 it seems that these uncertainties are conservative given how closely the integrals in the two figures track each other.

The uncertainties of the individual cells are estimated similarly: for each of the three layers by six segment cells in Table A1 we give the RMS velocities, the length of the segments, the DoF and effective number of sections and thickness for all cells. The resulting transport uncertainty for each of the layers is given in rows 4–6. These are copied into Table 1. The RMS velocity v′ can be obtained from the observed EKE along the section, which for the upper ocean just below the Ekman layer equals 0.021 m^2 s^{-2} dropping to 0.01 m^2 s^{-2} at 700 m depth with localized peaks to roughly twice these values in the PRIME eddy region at 20°W and over the Ridge. We will use v′ = 0.14 m s^{-1} for the top isopycnal layer and 0.1 m s^{-1} for the middle and bottom layers. There are an average of close to 150 profiles to 400 m depth dropping to ~80 at 700 m for each 10 km bin. The ADCP gets a profile every 3 min or equivalently 8 per bin for each transit. Being so close they are considered highly correlated so the effective number of data points or samples per 10 km box is more like 150/8 ~20 for the top layer and ~10 for the extension to the middle and bottom layers. These numbers may be on the conservative side since we assume perfect correlation for profiles obtained during

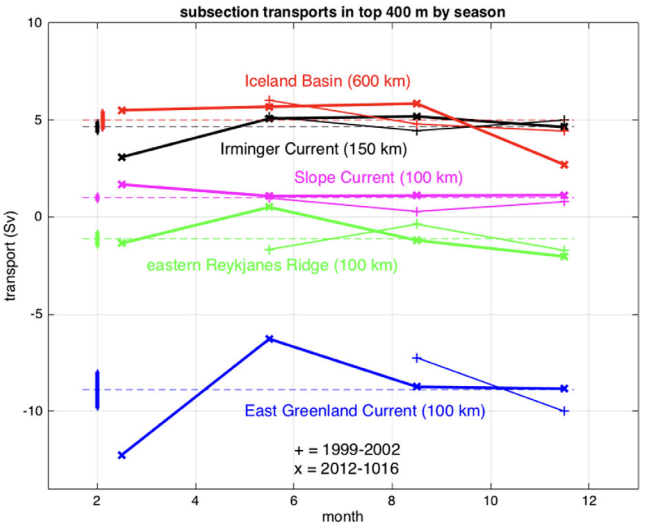

Figure A1. Transport in each of the principal flows as a function of season (months 1–3, 4–6, 7–9, and 10–12). The thin lines pertain to the 1999–2002 150 kHz data set, the thick lines to the 2012–2016 75 kHz data set. The dashed lines and bars on the left indicate the mean transport and corresponding standard errors for the corresponding groups. There are no wintertime data for the earlier data set.

a single transit through a box, and no allowance is made for fewer profiles from partial sections (which would be completely independent). The maximum possible number of sections is close to 50 since a Greenland-Denmark round trip takes 3 weeks and the data collection period spans 40 months. Weather and equipment failure account for the lack of more data. As in *Chafik et al.* [2014] we assume a decorrelation scale of 12 km so the DoF for each of the segments in the table is its length divided by this decorrelation scale. No assumptions are made about potential errors from the hydrographic extension. Had concurrent hydrography been available it is plausible that the density field would have attenuated some of the upper ocean eddy field in the deeper layers (assuming that a portion of the velocity variability is associated with baroclinic modes). The reduction in v′ from the surface to 700 m may reflect some of this attenuation. No DoF accrue from vertical averaging of velocity due to very high vertical coherence.

Another approach to estimating uncertainty examines each of the principal flows separately and by season: months 1–3, 4–6, 7–9, and 10–12. By considering just the top 400 m we can use the earlier data set as well. Figure A1 shows transport for each of the flows for all seasons where available. A couple of points can be made. First, there is no evident seasonal variation for any of the currents (with the possible exception of the Slope Current, which we know responds to winds [e.g., *Skagseth et al.*, 2004; *Berx et al.*, 2013]. Second, and as expected from Figure 6, there is no evident difference between the two data sets; the recent data (thin line) coincide with the earlier data (thick line). Taking all of these quarterly estimates for both data sets at equal value, the standard error for each of these are all less than 1 Sv except for the East Greenland Current (error bars at left end of each line). This puts a rather strong constraint on each of the flows, even for the 600 km wide Iceland Basin flow, which is the main branch of the North Atlantic Current toward the Nordic Seas.

The corresponding uncertainties for the heat and freshwater fluxes follow directly, as perturbations in the temperature or salinity fields have little effect compared to transport. That is why determining transport and its spatial structure accurately is so important. The uncertainties in Tables 2 and 3, not shown, are simply proportional to the transport uncertainties in the corresponding cell in Table 1.

Acknowledgments
First and foremost we are indebted to the Royal Arctic Line, and the officers of the Nuka Arctica for permission to install and operate an ADCP on the vessel, without which this study would not have been possible. We thank Professor Corinna Schrumm and the Bjerknes Center for Climate Research for the funds for the new 75 kHz ADCP that was installed in the Nuka Arctica in late 2012. We are profoundly grateful to Ms. S. Fontana for her careful editing, processing, and archival of all Nuka Arctica ADCP data. Without the care she puts into the processing, and especially the running calibration checks, this project would not have been possible. We are greatly indebted to Mr. Terje Hovland for his excellent support of the Nuka Artica operations. Support from the Institute of Marine Research for the ADCP operation on Nuka Arctica since 2012 is greatly appreciated. The XBT probes were mostly provided by NOAA and by Coriolis (France). Additional probes were funded by the Norwegian Research Council to Professor Are Olsen, Univ. of Bergen, Norway. Argo profiles are from the Coriolis data set (www.coriolis.eu.org) as extracted in January 2016 (http://doi.org/10.17882/42182#42349). The AVISO Ssalto/Duacs altimeter products were produced and distributed by the Copernicus Marine and Environment Monitoring Service (CMEMS) (http://www.marine.copernicus.eu). One of us (G.R.) was supported by INSU/CNRS through the SSS observing service. L.C. acknowledges funding through the iNcREASE project. Last, but not least, we express our sincerest thanks to the two anonymous reviewers who caught a couple of significant errors and shortcomings. Their comments have helped us to significantly improve the manuscript. We really truly appreciate their contributions.

References

Bacon, S. (1997), Circulation and fluxes in the North Atlantic between Greenland and Ireland, *J. Phys. Oceanogr.*, *27*, 1420–1435.
Bacon, S., and P. Saunders (2010), The deep western boundary current at Cape Farewell: Results from a moored current meter array, *J. Phys. Oceanogr.*, *40*, 815–829.
Beaird, N. L., P. B. Rhines, and C. C. Eriksen (2013), Overflow waters at the Iceland-Faroe ridge observed in multiyear seaglider surveys, *J. Phys. Oceanogr.*, *43*, 2334–2351, doi:10.1175/JPO-D-13-029.1.
Berx, B., B. Hansen, S. Østerhus, K. M. Larsen, T. Sherwin, and K. Jochumsen (2013), Combining in situ measurements and altimetry to estimate volume, heat and salt transport variability through the Faroe-Shetland channel, *Ocean Sci.*, *9*, 639–654, doi:10.5194/os-9-639-2013.
Bower, A. S., B. Le Cann, T. Rossby, W. Zenk, J. Gould, K. Speer, P. L. Richardson, M. D. Prater, and H.-M. Zhang (2002), Directly measured mid-depth circulation in the northeastern North Atlantic Ocean, *Nature*, *419*, 603–607.
Chafik, L., T. Rossby, and C. Schrum (2014), On the spatial structure and temporal variability of poleward transport between Scotland and Greenland, *J. Geophys. Res. Oceans*, *119*, 824–841, doi:10.1002/2013JC009287.
Childers, K. H., C. N. Flagg, and T. Rossby (2014), Direct velocity observations of volume flux between Iceland and the Shetland Islands, *J. Geophys. Res. Oceans*, *119*, 5934–5944, doi:10.1002/2014JC009946.
Childers, K. H., C. N. Flagg, T. Rossby, and C. Schrum (2015), Directly measured currents and estimated transport pathways of Atlantic water between 59.5°N and the Iceland-Faroes-Scotland Ridge, *Tellus, Ser. A*, *67*, 28,067, doi:10.3402/tellusa.v67.28067.

Daniault, N., et al. (2016), The northern North Atlantic circulation in the early 21st century, *Prog. Oceanogr.*, *146*, 142–158.
de Boisséson, E., V. Thierry, H. Mercier, G. Caniaux, and D. Desbruyères (2012), Origin, formation and variability of the Subpolar Mode Water located over the Ridge, *J. Geophys. Res.*, *117*, C12005, doi:10.1029/2011JC007519.
Dee, D. P., et al. (2011), The ERA-Interim reanalysis: Configuration and performance of the data assimilation system, *Q. J. R. Meteorol. Soc.*, *137*(656), 553–597.
de Jong, M. F., and L. de Steur (2016), Strong winter cooling over the Irminger Sea in winter 2014–2015, exceptional deep convection, and the emergence of anomalously low SST, *Geophys. Res. Lett.*, *43*, 7106–7113, doi:10.1002/2016GL069596.
Dickson, B., S. Dye, S. Jónsson, A. Köhl, A. Macrander, M. Marnela, J. Meincke, S. Olsen, B. Rudels, H. Valdimarsson, and G. Voet (2008), The overflow flux west of Iceland: Variability, origins and forcing, in *ASOF—Arctic-Subarctic Ocean Fluxes*, edited by R. R. Dickson et al., chap. 19, pp. 443–474, Springer, Berlin/Heidelberg, Germany.
Dobroliubov, S. A. (1997), Fresh water transport in the North Atlantic: Intercomparison of balance and direct estimates, in Abstract 08: Intercomparison and Validation of the Ocean-Atmosphere Flux Field. Euro. Geophys. Soc. 22nd General Assembly, Vienna Issue *15* (suppl. 2), p. C405.
Dunn, M. (2002), *A Description of the Barotropic Tide on Georges Bank Based Upon Five Years of Shipboard ADCP Measurements*, Stony Brook Univ. Sch. of Mar. and Atmos. Sci., New York.
García-Ibáñez, M. I., P. C. Pardo, L. I. Carracedo, H. Mercier, P. Lherminier, A. F. Ríos, and F. F. Pérez (2015), Structure, transports and transformations of the water masses in the Atlantic Subpolar Gyre, *Prog. Oceanogr.*, *135*, 18–36.
Girton, J. B., T. B. Sanford, and R. H. Kase (2001), Synoptic sections of the Denmark Strait Overflow, *Geophys. Res. Lett.*, *28*, 1619–1622, doi:10.1029/2000GL011970.
Hansen, B., K. M. H. Larsen, H. Hátún, R. Kristiansen, E. Mortensen, and S. Østerhus (2015), Increasing transports of volume, heat, and salt towards the Arctic in the Faroe Current 1993–2013, *Ocean Sci.*, *11*, 743–757, doi:10.5194/os-11-743-2015.
Heywood, K. J., E. L. McDonagh, and M. A. White (1994), Eddy kinetic energy of the North Atlantic subpolar gyre from satellite altimetry, *J. Geophys. Res.*, *99*, 22,525–22,539.
Holliday, N. P., S. Bacon, J. Allen, and E. L. McDonagh (2009), Circulation and transport in the Western Boundary Currents at Cape Farewell, Greenland, *J. Phys. Oceanogr.*, *39*, 1854–1870, doi:10.1175/2009JPO4160.1.
Häkkinen, S., and P. B. Rhines (2009), Shifting surface currents in the northern North Atlantic Ocean, *J. Geophys. Res.*,*114*, C04005, doi:10.1029/2008JC004883.
Ivers, W. D. (1975), The deep circulation in the northern North Atlantic, with special reference to the Labrador Sea, PhD thesis, 179 pp., Univ. of California, San Diego.
Jochumsen, K., M. Moritz, N. Nunes, D. Quadfasel, K. M. H. Larsen, B. Hansen, H. Valdimarsson and S. Jonsson (2017), Revised transport estimates of the Denmark Strait Overflow, *J. Geophys. Res. Oceans*, *122*, 3434–3450, doi:10.1002/2017JC012803.
Kalnay, E., et al. (1996), The NCEP/NCAR 40-year reanalysis project, *Bull. Am. Meteorol. Soc.*, *77*(3), 437–471, doi:10.1175/1520-0477(1996)077<0437:TNYRP>2.0.CO;2.
Knutsen, Ø., H. Svendsen, S. Østerhus, T. Rossby, and B. Hansen (2005), Direct measurements of the mean flow and eddy kinetic energy structure of the upper ocean circulation in the NE Atlantic, *Geophys. Res. Lett.*, *32*, L14604, doi:10.1029/2005GL023615.
Krauss, W. (1986), The North Atlantic Current, *J. Geophys. Res.*, *91*, 5061–5074.
Lavender, K. L., R. E. Davis, and W. B. Owens (2000), Direct velocity measurements describe a new circulation regime in the Labrador and Irminger Seas, *Nature*, *407*, 66–69.
Lavender, K. L., W. B. Owens, and R. E. Davis (2005), The mid-depth circulation of the subpolar North Atlantic Ocean as measured by subsurface floats, *Deep Sea Res., Part I*, *52*, 767–785.
Locarnini, R. A., et al. (2013), World Ocean Atlas 2013, vol. *1*, Temperature, edited by S. Levitus, Ed., A. Mishonov Technical Ed.; NOAA Atlas NESDIS 73, 40 pp.
Macrander, A., U. Send, H. Valdimarsson, S. Jonsson, and R. H. Käse (2005), Interannual changes in the overflow from the Nordic Seas into the Atlantic Ocean through Denmark Strait, *Geophys. Res. Lett.*, *32*, L06606, doi:10.1029/2004GL021463.
Martin, A. P., I. P. Wade, K. J. Richards, and K. J. Heywood (1998), The PRIME eddy, *J. Mar. Res.*, *56*, 439–462.
Mastropole, D., R. S. Pickart, H. Valdimarsson, K. Våge, K. Jochumsen, and J. Girton (2017), On the hydrography of Denmark Strait, *J. Geophys. Res. Oceans*, *122*, 306–321, doi:10.1002/2016JC012007.
McCartney, M. S., and C. Mauritzen (2001), On the origin of warm inflow into the Nordic Seas, *Prog. Oceanogr.*, *51*, 125–214.
McCartney, M. S., and L. D. Talley (1984), Warm-to-cold water conversion in the Northern North Atlantic Ocean, *J. Phys. Oceanogr.*, *14*, 922–935.
Mercier, H., et al. (2015), Variability of the meridional overturning circulation at the Greenland-Portugal OVIDE section from 1993 to 2010, *Prog. Oceanogr.*, *132*, 250–261.
Riser, S. C., L. Ren, and A. Wong (2008), Salinity in Argo, *Oceanography*, *21*, 56–67.
Robson, J., P. Ortega, and R. Sutton (2016), A reversal of climatic trends in the North Atlantic since 2005, *Nat. Geosci.*, *9*, 513–517, doi:10.1038/ngeo2727.
Sarafanov, A., A. Falina, H. Mercier, A. Sokov, P. Lherminier, C. Gourcuff, S. Gladyshev, F. Gaillard, and N. Daniault (2012), Mean full-depth summer circulation and transports at the northern periphery of the Atlantic Ocean in the 2000s, *J. Geophys. Res.*, *117*, C01014, doi:10.1029/2011JC007572.
Sherwin, T. J., M. O. Williams, W. R. Turrell, S. L. Hughes, and P. I. Miller (2006), A description and analysis of mesoscale variability in the Faroe-Shetland Channel, *J. Geophys. Res.*, *111*, C03003, doi:10.1029/2005JC002867.
Skagseth, Ø, K. A. Orvik, and T. Furevik (2004), Coherent variability of the Norwegian Atlantic Slope Current derived from TOPEX//ERS altimeter data, *Geophys. Res. Lett.*, *31*, L14304. doi:10.1029/2004GL020057
Søiland, H., M. D. Prater, and T. Rossby (2008), Rigid topographic control of currents in the Nordic Seas, *Geophys. Res. Lett.*, *35*, L18607, doi:10.1029/2008GL034846.
Trenberth, K. E., and J. T. Fasullo (2008), An observational estimate of inferred ocean energy divergence, *J. Phys. Oceanogr.*, *38*, 984–999.
Våge, K., R. S. Pickart, V. Thierry, G. Reverdin, C. M. Lee, B. Petrie, T. A. Agnew, A. Wong, and M. H. Ribergaard (2009), Surprising return of deep convection to the subpolar North Atlantic Ocean in winter 2007–2008, *Nat. Geosci.*, *2*, 67–72, doi:10.1038/NGEO382.
Våge, K., R. S. Pickart, A. Sarafanov, Ø. Knutsen, H. Mercier, P. Lherminier, H. M. van Aken, J. Meincke, D. Quadfasel, and S. Bacon (2011), The Irminger Gyre: Circulation, convection, and interannual variability, *Deep Sea Res., Part I*, *58*, 590–614.
Wade, I. P., and K. J. Heywood (2001), Tracking the PRIME eddy using satellite altimetry, *Deep Sea Res., Part II*, *48*(4–5), 725–737.
Wang, Y.-H., L.-Y. Chiao, K. M. M. Lwiza, and D.-P. Wang (2004), Analysis of flow at the gate of Taiwan Strait, *J. Geophys. Res.*, *109*, C02025, doi:10.1029/2003JC001937.

Wijffels, S. E. (2001), Ocean transport of fresh water, in *Ocean Circulation and Climate*, edited by G. Siedler, J. Church, and J. Gould, chap. 6.2, *Int. Geophys. Ser.*, *77*, 715 pp.

Willis, J. (2010), Can in situ floats and satellite altimeters detect long-term changes in Atlantic Ocean overturning? *Geophys. Res. Lett.*, *37*, L06602, doi:10.1029/2010GL042372.

Worst, J. S., K. A. Donohue, and T. Rossby (2014), A comparison of vessel-mounted acoustic Doppler current profiler and satellite altimeter estimates of sea surface height and transports between New Jersey and Bermuda along the CMW Oleander route, *J. Atmos. Oceanic Technol.*, *31*, 1422–1433.

Zweng, M. M., et al. (2013), World Ocean Atlas 2013, vol. 2, Salinity, edited by S. Levitus, Ed., A. Mishonov Technical Ed., NOAA Atlas NESDIS 74, 39 pp.